Chemical Engineering Journal 160 (2010) 852–864

Contents lists available at ScienceDirect

Chemical Engineering Journal

journal homepage: www.elsevier.com/locate/cej

Analysis and multi-criteria design optimization of geometric characteristics of grooved micromixer

Cesar A. Cortes-Quiroz[a,*], Alireza Azarbadegan[a], Mehrdad Zangeneh[a], Akira Goto[b]

[a] University College London, Department of Mechanical Engineering, UK
[b] Ebara Research Co. Ltd., Japan

ARTICLE INFO

Article history:
Received 9 August 2009
Received in revised form 20 January 2010
Accepted 16 February 2010

Keywords:
Grooved micromixer
CFD
Multi-objective optimization
Design of experiments
Surrogate modelling
Genetic algorithm

ABSTRACT

Computational fluids dynamics (CFDs) and numerical optimization techniques are applied in an integrated methodology to explore the effects of different geometric characteristics on fluid mixing in a staggered herringbone micromixer (SHM). To quantify the mixing intensity in the mixer a mixing index is defined on the basis of the intensity of segregation of the mass concentration on a cross-section plane in the mixing channel. Four geometric parameters, i.e., aspect ratio of the mixing channel, ratio of groove depth to channel height, ratio of groove width to groove pitch and the asymmetry factor (offset) of groove, are the design variables initially selected for optimization, then two more parameters, i.e., angle of the groove and number of grooves per channel section, are evaluated. The whole optimization is conducted with a multi-objective approach for which the mixing index at the outlet section and the pressure drop in the mixing channel are the performance criteria used as objective functions. The Pareto front of designs with the optimum trade-off, maximum mixing index with minimum pressure drop, is obtained.

1. Introduction

Microfluidics systems share properties such as laminar flows, reduced thermal gradients and small sample/reagent volumes that help for effective process control and reproducibility. These advantages have been exploited to build microfluidic devices for lab-on-a-chip applications [1] where functions such as separation, mixing, reaction, synthesis and analysis are performed. This microdevice concept and technology has developed rapidly and has a growing use in biological [2] and chemical [3,4] applications: sorting of cells, drug delivery, chemical and enzyme reactions, synthesis of nucleic acids and analysis of DNA and proteins. In most microfluidic applications, e.g. fast chemical reactions, DNA separation and amplification, the performance of the microfluidic system is governed by its mixing efficiency. Therefore, among microfluidic devices, micromixers have been developed to achieve fast mixing and they play an important role in Bio-Micro-Electro-Mechanical Systems (BioMEMS), microheat exchangers, microreactors and micro-total-analysis systems (μ-TAS).

In microfluidic devices, fluid flows are characterized by low values of Reynolds number at which the flow is laminar and molecular diffusion is the dominant mixing mechanism. For the scales of typical microchannels under practical flow conditions, mixing by diffusion is a very slow process and consequently it increases the length of microchannels and time required for complete mixing. Microfluidic mixing can be improved by stretching and folding of fluids which redistributes the fluids, decreases the diffusion path and increases the interfacial area between the fluids, which in turn increases the probability for solute transport between fluids and, therefore, the mixing performance. Design of micromixers is based on the achievement of three basic processes of fluids mixing: molecular diffusion, stretching and folding and break up [5]. Various micromixer designs have been reported in the literature and they can be classified into active and passive micromixers [6,7]. Active micromixers perturb the flow field either by using moving parts or an external source of energy such as an electric field, magnetic field, acoustic waves or varying pressure gradients. Passive micromixers do not use external actuation except a pressure head or pump to drive flows into the microfluidic system where mixing is achieved by creating a transverse flow through modification of their geometries.

In general, active micromixers can stir up fluids better than passive micromixers, but they all share the drawback of their complexity of fabrication or operation. Therefore, passive micromixers have been preferred in most applications due to their simple design, easiness of fabrication and integration compared with their active counterparts and they are frequently adapted in the development of integrated microfluidic chips.

* Corresponding author. Tel.: +44 0 2076793997; fax: +44 0 2073880180.
E-mail addresses: cesar.cortes@ucl.ac.uk, c.cortesqurz@meng.ucl.ac.uk (C.A. Cortes-Quiroz).

1385-8947/$ – see front matter © 2010 Elsevier B.V. All rights reserved.
doi:10.1016/j.cej.2010.02.029

One of the passive methods to enhance mixing process is to place microstructured objects on one or more walls of the channel. One of these designs, the staggered herringbone micromixer (SHM) [8], has been found to give good mixing performance at low Reynolds numbers (Re < 100). A transverse flow is produced through the asymmetric herringbone shaped grooves on the floor of the channel to generate two counter-rotating helical flows that create a chaotic flow profile due to the alternated asymmetry of the herringbones along the length of the micromixer.

Several theoretical, experimental and numerical studies have been carried out on the SHM with the aim of understanding the mixing mechanism and the effect of various geometrical parameters on the mixing quality. Stroock and McGraw [9] approximated the complex three-dimensional flow field using a two dimensional lid-driven cavity model that was tuned to provide qualitative agreement to experimental data and studied the effect of varying two geometric parameters: the asymmetry factor of the groove and the number of grooves in each cycle; Liu et al. [10] studied the influence of different fluid properties and a large concentration gradient on mixing at Re = 1 and 10 for a fixed geometry; Aubin et al. [11,12] investigated numerically the effect of three geometric parameters: the groove depth, the groove width and the number of grooves per cycle, using a particle tracking method to visualize and quantify the mixing performance; Kang and Kwon [13] applied a coloured particle tracking method to study numerically the mixing performance of three types of grooved micromixers including the SHM; Yang et al. [14] studied the effects of varying herringbone groove offset, depth, and angle, as well as the ratio of inlet channel width to mixing channel width by applying CFD to nine configurations defined with an array given by the Taguchi method; Li and Chen [15] used the Lattice Boltzmann method to study numerically the effect on mixing performance of the asymmetry factor and the number of grooves per half-cycle; Hassel and Zimmerman [16] presented a numerical study of the flow through the SHM to characterize the effect of the grooves on moving fluid across the channel, in particular of the groove depth in Re range 0–15 and of the number of grooves per half-cycle; Lynn and Dandy [17] evaluated numerically the generation of helical flows in the slanted groove micromixer (SGM) and its optimization, i.e., the increment of transverse flow, by varying the ratio of the length of the grooves to the neighbouring ridge for a given groove depth and channel aspect ratio, and discussed the implications of translating the optimized parameters to the SHM design; Ansari and Kim [18] used a numerical procedure that combines three-dimensional Navier–Stokes analysis and a numerical optimization technique, the response surface method (RSM), to enhance mixing performance by optimizing the groove using the ratio of groove depth to channel height and angle of the groove; Singh et al. [19] introduced a new simplified formulation of the mapping method [20] to make it much simpler to implement and applied the method to optimize three micromixer designs including the SHM for which groove depth and number of grooves per half-cycle were used as parameters; very recently, Cortes-Quiroz et al. [21,22] presented a multi-criteria design optimization methodology for micromixers based on the integration of CFD with numerical optimization techniques and applied it for the optimization of four geometries of the SHM to obtain good mixing performance with low pressure loss.

Definitely, mixing in the SHM can be effectively increased by optimizing the shape of the grooves and channel. As cited above, previous work has already investigated on the effects of geometric parameters on mixing but these studies do not exactly 'optimize' but 'improve' the micromixers design to enhance mixing performance since they do not cover the whole design space and work basically through parametric investigation on discrete number of geometries. Few attempts have systematically used automatic optimization techniques for designing micromixers and almost all of them applied a single criterion optimization with mixing performance as the only objective. However, in most problems of practical interest multi-objective criteria need to be met, e.g. mixing vs. pressure loss, energy consumption or dissipation, residence time.

In this paper, a design and multi-objective optimization methodology is applied to the SHM. It systematically integrates CFD with an optimization strategy based on the use of design of experiments (DOE), surrogate modelling (SM) and multi-objective genetic algorithm (MOGA) techniques. The study is based on and complements the work of Cortes-Quiroz et al. [22]. The effects on mixing and pressure drop of six selected geometric parameters of the SHM have been evaluated and the parameters optimized accordingly. The goal of the optimization is to obtain SHM configurations that provide maximum mixing index with lowest pressure drop.

2. Numerical analysis

A schematic diagram of the SHM channel is shown in Fig. 1 which displays the geometric characteristics considered in this study. For all the models prepared in this study, the mixing channel length is 3 mm. It is important to mention that notation in this study differs from previous studies on SHM geometries; 'h' refers to the height of the inlet and mixing channels, i.e., dimension 'h' does not include the depth of the groove, and 'λ' refers to groove pitch in direction perpendicular to the walls of the grooves, i.e., dimension 'λ' is not the pitch of the grooves at the intersection with the channel walls (axial pitch). This definition of groove pitch has only be found in [22] and it is particularly important to use it in this paper to avoid the interaction effects between parameters w_g/λ and θ since variation of the latter in a fixed axial pitch design implies change in the channel width w_g which means these parameters would not be independent of each other. Also, the distribution of the grooves in the different models prepared for this study does not have a break in the space between half-cycles of grooves, i.e., the groove pitch is invariable in the whole channel length. The parameter N_g can change the number of grooves in the fixed 3 mm channel length used in this study; nevertheless, the creation of the SHM models in this study has taken into account no groove is abruptly cut at the outlet end nor it is too close to the outlet end (<150 μm) and CFD investigation has been made to confirm there is not significant influence on the results.

The analysis of the transport process in the SHM designs is performed numerically. Flow field and mixing are computed using ANSYS CFX-11 [23], commercial modelling software based on the finite volume method. The flow has been defined as viscous, isothermal, incompressible, laminar and in steady state, for which the code solves the continuity equation, the momentum equation (Navier–Stokes) and the species convection-diffusion equation.

Since numerical simulations are not free from numerical diffusion error which arises from the discretization of the advection terms in the Navier–Stokes equations, these terms in each equation are discretized with a second order differencing scheme which minimizes numerical diffusion in the results. The condition of convergence of simulations is the root-mean square (rms) normalized residual of mass fraction falling below 1×10^{-5}.

For the boundary conditions, a normal velocity is defined and given the same value at both inlets for the fluids to come into contact and start mixing in the T-junction, a constant pressure (gauge pressure = 0) is specified at the outlet boundary and the non-slip condition is used on the walls. Water at 25 °C (dynamic viscosity, $\mu_{H_2O} = 8.899\text{E}-04$ kg/m s; density, $\rho_{H_2O} = 997$ kg/m^3) and Ethanol (dynamic viscosity, $\mu_{C_2H_{60}} = 1.197\text{E}-03$ kg/m s; density, $\rho_{C_2H_{60}} = 789$ kg/m^3) are the working fluids used for mixing where the kinematic diffusivity of ethanol in water is 8.4E−10 m^2/s, the

w	Width of the channel
h	Height of the channel
w_g	Width of the groove
d_g	Depth of the groove
γ	Angle of intersection of groove and channel axis
θ	Angle of groove
b	Asymmetry factor (offset)
λ	Groove pitch
N_g	Number of grooves per half cycle

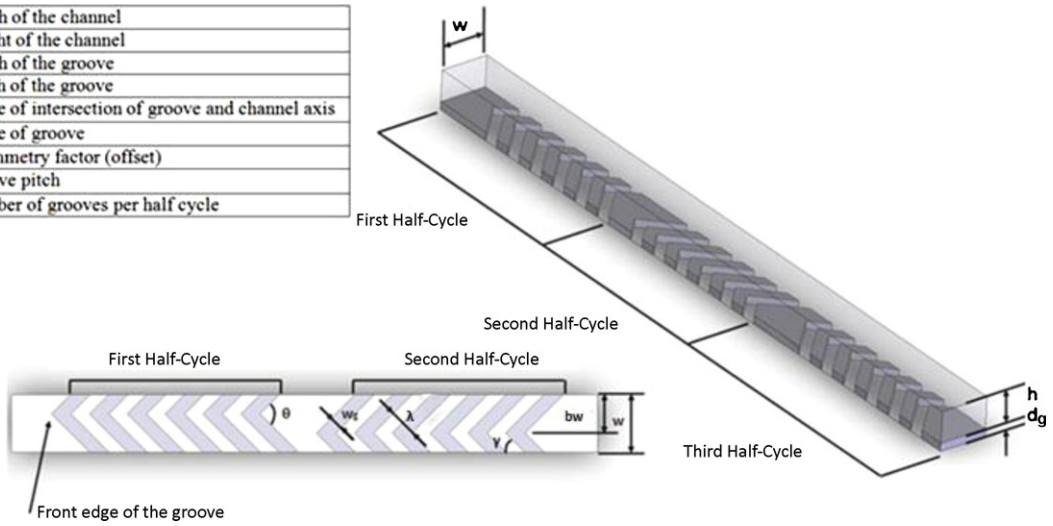

Fig. 1. Geometric characteristics of the SHM for parameterization and optimization.

boundary conditions for the species balance are mass fraction equal to 0 at the inlet where pure water is fed and equal to 1 at the inlet where Ethanol is fed.

GRIDGEN 15.1 [24] is used to build the geometries of SHM designs and to make grids for their full domains. A high quality mesh is essential for the accuracy of results, in particular for analyzing the effect of geometry on mixing. A structured grid of hexahedral elements is made in the models and arranged to provide sufficient resolution for boundary layers near the fluid–solid interface (walls) and sufficient number of nodes at the corners. Two mesh zones of the herringbone are shown in Fig. 2. To obtain mesh-independent results from the simulations, a preliminary mesh size sensitivity analysis was carried out to find the interval of mesh size at which convergence is reached for the computation of mixing quality and pressure loss. The size of the mesh cells for all the SHM models (inlet channels length = 0.5 mm, mixing channel length = 3 mm) prepared for this study resulted in the range of 0.7–4.5 μm approximately for a mesh density in the range of 3.55–5.3 million hexahedra cells.

For the optimization process that is described in next section, the grid distribution and the slight geometry variation of the design models make comparable the level of any remaining numerical diffusion in the results. Therefore, finding the optimum geometries of the micromixer is possible with the grid quality in models domains, the discretization scheme of Navier–Stokes equations and the numerical optimization techniques employed in the paper.

3. Optimization methodology

Fig. 3 shows the flowchart diagram of the analysis and optimization process for the optimization of the micromixer. The process was explained by Cortes-Quiroz et al. [21,22] and here it will be described more straightforward to define some parameters and techniques to be used in the application of the methodology to the shape optimization of the SHM design in Section 4.

The first step is to define what performance parameters (objective functions) are going to be optimized and to select the design parameters with a range of variation for the optimization study. Then, the design of experiments (DOE) method is used to create the experimental table of designs points which correspond to a number of geometries in the micromixer design space defined by the ranges of the design parameters. CFD simulations are used on these geometries to compute the performance parameters. Once the flow field is solved for all the designs a surrogate modelling (SM) technique can be used to define approximated response functions or surfaces that describe the correlation between the performance parameters and the design parameters. The accuracy of the response surface is a key condition in the design process since it can be used to carry out a sensitivity analysis that can be used to find the most critical design parameters and to change the design geometry accordingly to improve its performance [18], and in turn it defines the accuracy of the final optimization step resulting from applying a multi-objective genetic algorithm (MOGA) on the response surface. The application of the MOGA on the response surface reduces dras-

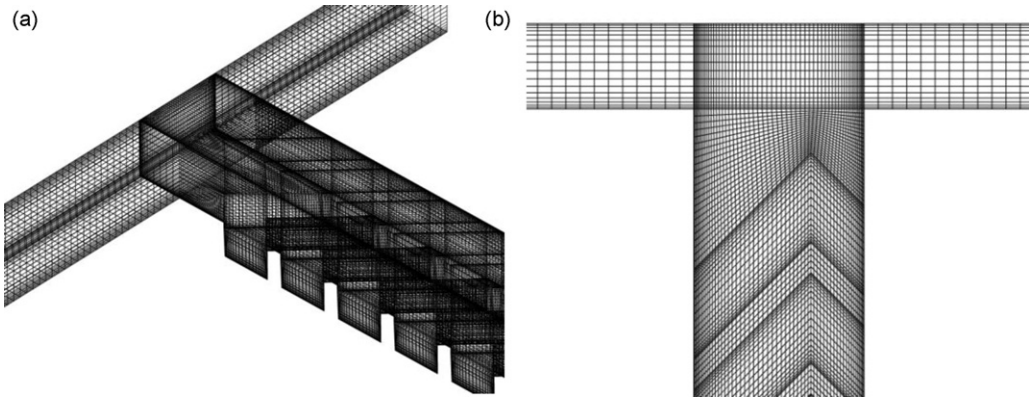

Fig. 2. Mesh details of T-junction of the SHM: (a) isometric view (b) top view.

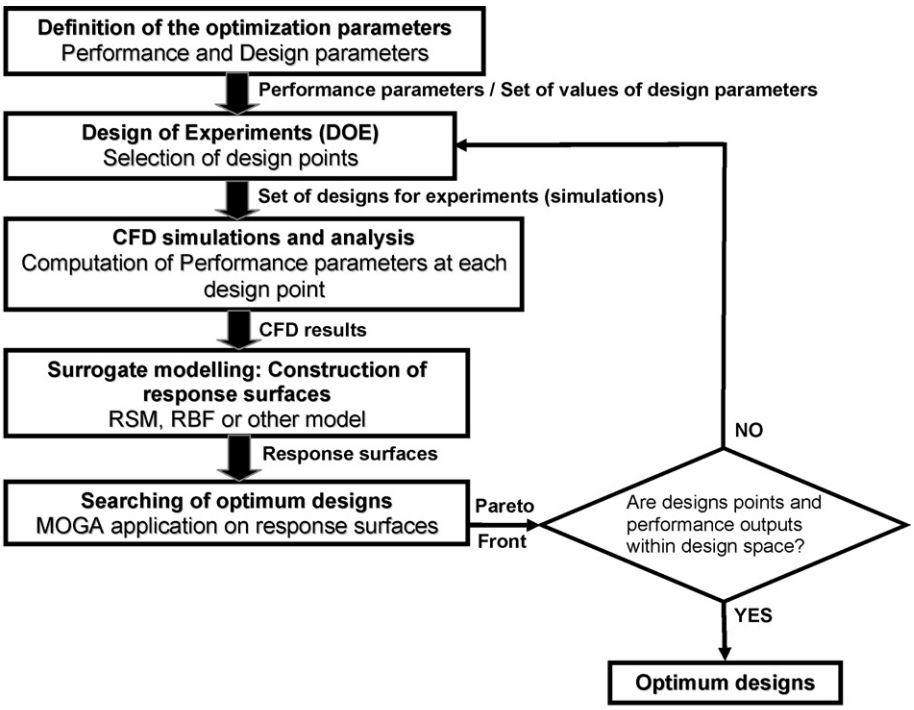

Fig. 3. Flowchart of the analysis and optimization process.

tically the computational cost of applying it on a great number of designs that might have to be solved first by CFD. The optimization procedure finally gives the optimum boundary of designs, i.e., the Pareto front (Pf), that reveals the trade-offs between the performance parameters in the design space.

3.1. Definition of the parameters for the optimization study

The performance parameters defined for this study are the mixing quality and the pressure drop in the channel. In order to measure and compare the mixing quality using the outputs from CFD code, a mixing index is defined based on mass concentration distribution. In this study, the definition of mixing index is based on the intensity of segregation introduced by Danckwerts [25] and is calculated by Eq. (1):

$$Mi = 1 - \sqrt{\frac{\int_A (c - \bar{c})^2 dA}{A\bar{c}(1 - \bar{c})}} \quad (1)$$

where c is the concentration distribution at the selected cross-section plane (in this study, it is the outlet plane at the end of the mixing channel), $\bar{c}$ is the averaged value of the concentration field on the plane and A is the area of the plane. Mi reaches a value of 0 for a complete segregated system and a value of 1 for the homogeneously mixed case. The mass concentration information from CFD analyses is used in Eq. (1).

The second performance parameter is the pressure loss in the mixing channel which is computed by the difference between the area weighted average of total pressure on the outlet plane and on a cross-section plane at the inlet of the mixing channel.

For the selection of the design parameters, conclusions from previous work on mixing in the SHM (cited in Section 1) and a sensitivity analysis of the influence of design parameters on the mixing index led Cortes-Quiroz et al. [22] to use four design parameters for the optimization: aspect ratio of the mixing channel, w/h, ratio of groove depth to channel height, d_g/h, ratio of groove width to groove pitch, w_g/λ, and the asymmetry factor, b, with the next geometric features fixed: width of the mixing channel, w = 200 μm, groove pitch, λ = 100 μm, angle of the groove, $\theta = 90^\circ$, number of grooves per half-cycle, $N_g = 6$, and width of inlet channels, D = 100 μm. This multi-criteria optimization is brought further in this paper using the optimum geometry obtained by Cortes-Quiroz et al. [22] as a reference design and optimizing then the following parameters: ratio of groove depth to channel height, d_g/h, ratio of groove width to groove pitch, w_g/λ, angle of the groove, θ, and number of grooves per half-cycle, N_g, whereas other geometric dimensions are kept fixed.

Table 1 shows the design parameters values used in the first multi-criteria optimization study of the SHM [22] and Table 2 shows similar information for the study completed in this paper.

3.2. Design of experiments (DOE)

DOE method defines a subset of design points (for carrying out experiments or simulations) from the design space which is representative enough to evaluate the influence of designs parameters on performance parameters.

The Taguchi method [26] is used in this study. It is based on orthogonal array (OA) of experiments that gives much reduced

Table 1
Design parameters of the SHM designs used with first DOE.

Levels	Factors[a]			
	A (w/h)	B (d_g/h)	C (w_g/λ)	D (b)
1	1.60	0.25	0.25	0.55
2	2.40	0.50	0.50	0.70
3	3.20	0.75	0.75	0.85

[a] Factors are defined as follows: (A) aspect ratio of the mixing channel. (B) Ratio of groove depth to mixing channel height. (C) Ratio of groove width to groove pitch. (D) Asymmetry factor.

Table 2
Design parameters of the SHM designs used with second DOE.

Levels	Factors[a]			
	A (d_g/h)	B (w_g/λ)	C (θ°)	D (N_g)
1	0.30	0.30	70	5
2	0.55	0.525	90	6
3	0.80	0.75	110	7

[a] Factors are defined as follows: (A) Ratio of groove depth to mixing channel height. (B) Ratio of groove width to groove pitch. (C) Angle of the groove. (D) Number of grooves per half-cycle.

variance for the experiment with optimum settings of design parameters. Applying this method, the number of experiments (simulations) can be reduced significantly by using the orthogonal arrays which provide a set of well balanced experiments, and the sensitivity of the design parameters on the mixing index can be analyzed through the Taguchi's signal-to-noise ratios (S/N) which can also be used to predict the optimum values of the parameters. For this sensitivity analysis, variables are divided into design parameters and source of noise (noise factor) and the design of experiments (DOE) is used to determine the design parameters which minimize the effect of noise factors on performance characteristics, for which Taguchi method uses the loss function and S/N ratio. When a response never has a negative value and its target value is ideally zero, these are referred to as smaller-the-better characteristics. Since the target response of the mixing index is ideally zero (see integrand in the square root of Eq. (1)), the static Taguchi analysis for the problem with the smaller-the-better character is performed for having an initial estimation of optimum values of design variables.

The S/N ratio is a log function and in this study it is defined to use output values from simulations. Therefore, the square of the standard deviation of concentration at the outlet of micromixer is calculated by using Eq. (2):

$$\sigma^2 = \frac{1}{n}\sum_{i=1}^{n}(c_i - c_\infty)^2 \tag{2}$$

where c_i is the concentration distribution of one of the fluids at the ith cell on the outlet, c_∞ is the concentration of complete mixing and n is the number of cells defined by the mesh on the outlet plane. Then, the signal-to-noise ratio with the smaller-the-better character can be evaluated by Eq. (3):

$$\frac{S}{N} = -10\log\sigma^2 \tag{3}$$

For four design parameters with three levels each (see Tables 1 and 2), the orthogonal array L_{27} is used to define 27 experiments or design points; the columns in the original L_{27} table for the factors of interaction between the four factors are not considered. This orthogonal array is shown in Table 3.

3.3. CFD simulations and analysis

CFD simulations are prepared and solved for the 27 SHM designs defined by the DOE. The details of the geometries modeled and meshes used as well as the numerical simulations settings are described in Section 2.

3.4. Surrogate modelling (SM). Construction of response surfaces

The values of design parameters X_i of the SHM designs defined in the DOE matrix (Table 3) and the performance parameters P_j (mixing index, pressure drop) outputs from CFD simulations of the DOE designs are used to construct approximated functions or response surfaces:

$$P_j = p_j(X_i), \quad i = 1 \text{ to } N, \quad j = 1 \text{ to } M \tag{4}$$

where N is the number of design parameters and M is the number of performance parameters. There are several surrogate modelling techniques that can be used to construct the response surface by interpolating the data and to optimize the objective function on the response surface. In the present study they are only used for the construction of the response surfaces whereas the optimization on the response surface is made by a multi-objective genetic algorithm (MOGA) according to Section 3.5.

Two surrogate modelling techniques have been used: response surface methodology (RSM) [27] and radial basis function (RBF) [28,29].

The RSM normally approximates the objective functions by polynomial based response surfaces whose order must be chosen first. In the present study, the response model is assumed as a second order polynomial function that can be expressed as

$$P_j = \alpha_0 + \sum_{i=0}^{N}\alpha_i X_i + \sum_{i=0}^{N}\alpha_{ii}X_i^2 + \sum_{i\neq j}^{N}\alpha_{ij}X_iX_j \tag{5}$$

where N is the number of design variables and the unknown polynomials coefficients $\alpha_0, \alpha_i, \alpha_{ii}$ and α_{ij} are obtained from a standard least-square regression applied on calculated responses at the design points provided by the DOE; the number of coefficients is $(N+1)\times(N+2)/2$.

The RBF is a two-layered neural network with a hidden layer of radial units and an output layer of linear units. The hidden layer consists of a set of radial basis functions that act as activation functions whose response varies with the distance between the input and the centre; the distance between two points is given by the difference of their coordinates and by a set of parameters. The RBF is fairly compact, where the linear nature of the radial basis functions reduces computational cost to have a reasonably fast training. The

Table 3
Orthogonal array L_{27}.

Exps.[a]	Factors[b]			
	A	B	C	D
1	1	1	1	1
2	1	1	2	2
3	1	1	3	3
4	1	2	1	2
5	1	2	2	3
6	1	2	3	1
7	1	3	1	3
8	1	3	2	1
9	1	3	3	2
10	2	1	1	2
11	2	1	2	3
12	2	1	3	1
13	2	2	1	3
14	2	2	2	1
15	2	2	3	2
16	2	3	1	1
17	2	3	2	2
18	2	3	3	3
19	3	1	1	3
20	3	1	2	1
21	3	1	3	2
22	3	2	1	1
23	3	2	2	2
24	3	2	3	3
25	3	3	1	2
26	3	3	2	3
27	3	3	3	1

[a] Experiments which correspond to the design models used in CFD simulations.
[b] Factors are defined in Tables 1 and 2.

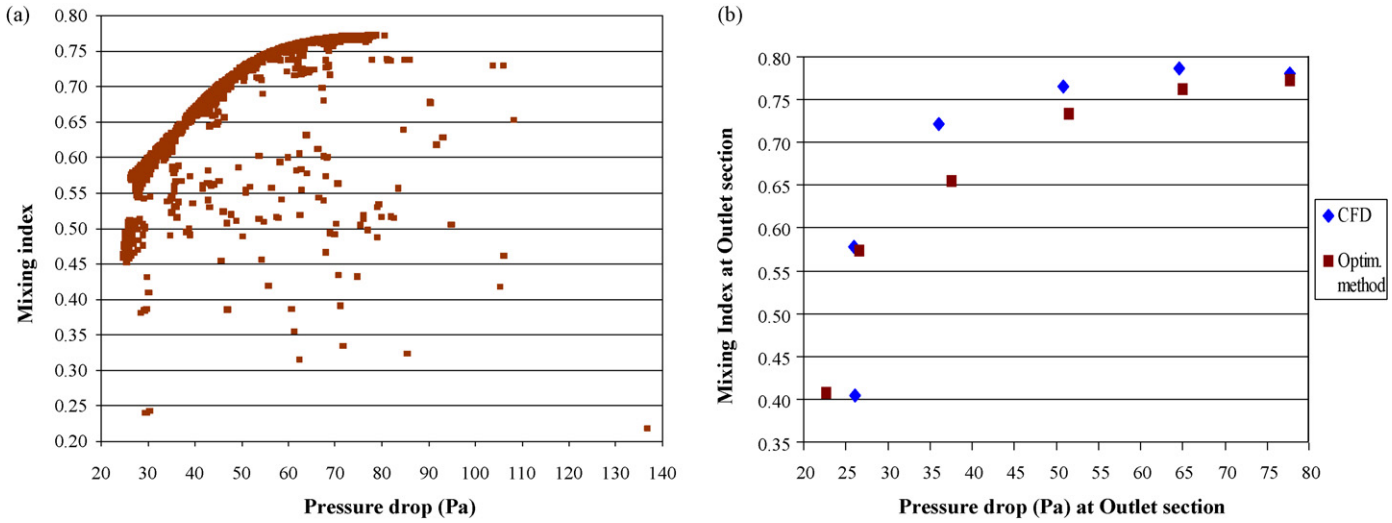

Fig. 4. Results from application of NSGA-II optimization algorithm on response surfaces built by RBF method: (a) scatter of iterations history and (b) scatter of six samples from Pareto front comparing CFD with optimization method results (from [22]).

model for the function is a linear combination of a set of weighted basis functions; the prediction capacity of the network is stored in the weights which can be obtained from a set of training patterns. This process is equivalent to finding a surface in multidimensional space that provides the best fit to the training data, which is then used to interpolate the test data.

To measure the uncertainty of the response surface models a regression analysis is done [30] to determine the values of two error factors: R^2 (the ratio of the model sum of squares to the total sum of squares) and R^2_{adj} (R^2 adjusted to the number of parameters in the model). A value of R^2_{adj} in the range 0.9–1.0 indicates that the response surface model predicts accurately the response values.

3.5. Searching of optimum designs

Numerical optimization methods are efficient tools for finding correlations between geometrical parameters and device performance outcomes from CFD and optimizing their combination. They have been applied to optimization problems in areas such as aerodynamic optimization [31], mechanical and structural design [32].

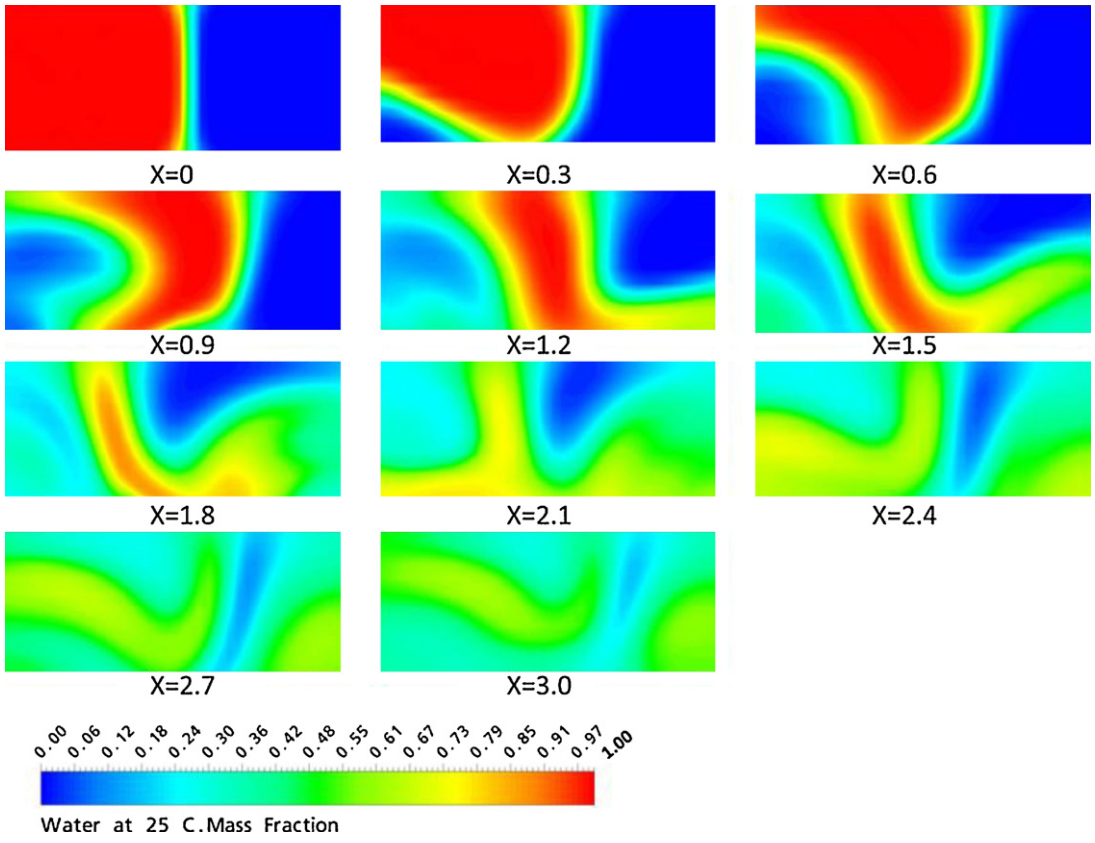

Fig. 5. Mass fraction contours on cross-section planes of mixing channel of optimum design RBF pf19 from first part of optimization study.

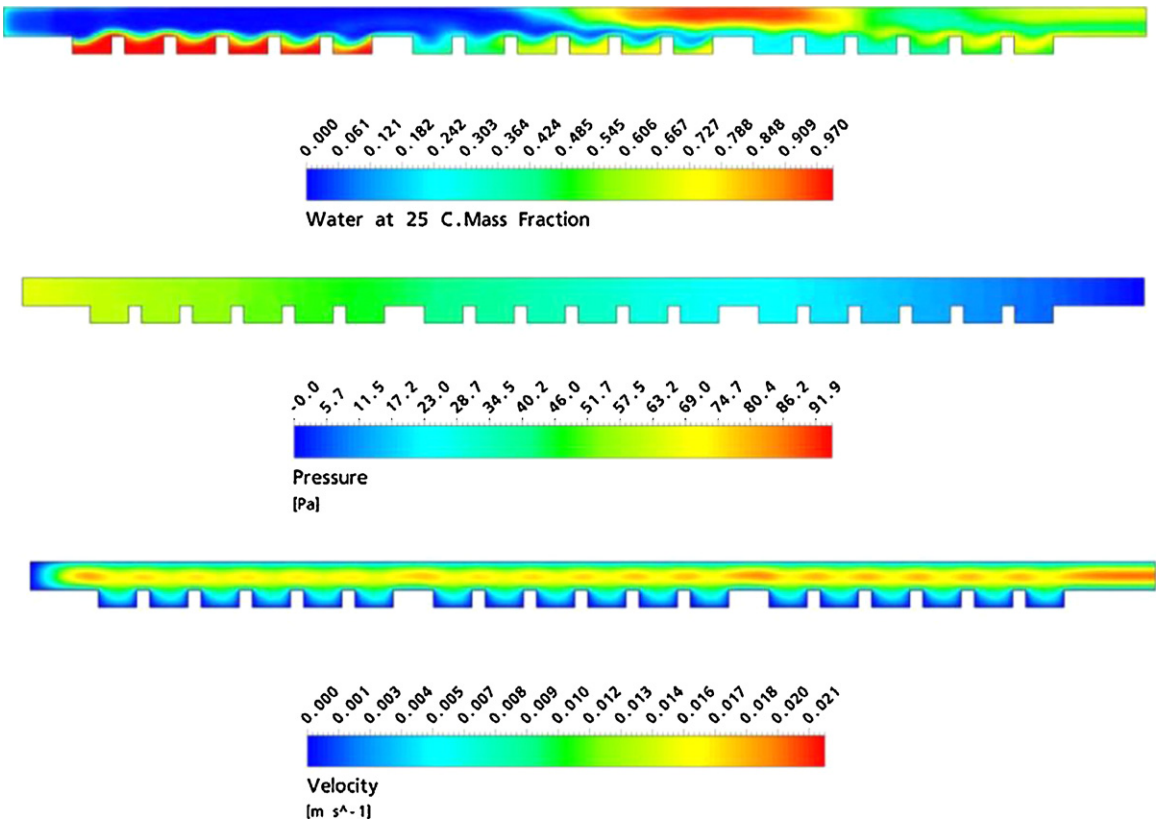

Fig. 6. Mass fraction, pressure and velocity contours on symmetrical vertical plane of mixing channel of optimum design RBF pf19 from first part of optimization study.

Since micromixing optimization is a non-linear problem, i.e., a multipeak problem, an exploratory technique has to be used for seeking the global optimum; it evaluates designs throughout the parameter space and only makes use of the computation of the objective functions values. In this study, a genetic algorithm has been used due to its capacity to be implemented to solve multi-objective optimization problems. This multi-objective genetic algorithm (MOGA) can converge to a population composed of individuals that belong to the Pareto front of the solutions. To avoid the high number of evaluations of the objective function required to reach an optimum configuration, the actual objective functions are replaced by the approximated functions (response surfaces) that are constructed by surrogate modelling.

The non-dominated sorting genetic algorithm (NSGA-II) [33] has been used in this study due to its effectiveness working with non-linear problems and in finding the optimum solutions of Pareto front. The NSGA-II is applied on the response surfaces with the following initial parameters values: population size = 26, number of generations = 100, crossover probability = 0.9, crossover distribution index = 20 and mutation distribution index = 100. These values were changed systematically to reach number of generations of 500, crossover distribution of 50 and mutation distribution index of 250 with the purpose of evaluating the singularity of the convergence of predicted optimum designs test. No constraints were applied on the design and performance parameters. The convergence was confirmed and the initial parameters values were used to obtain the optimum designs geometries. The application pursues the maximization of the mixing index and the minimization of the pressure drop.

4. Results and discussion

The first part of this study has been the application of the optimization methodology on a set of designs defined by the design parameters shown in Table 1 and organized in the orthogonal array L_{27} (Table 3). Cortes-Quiroz et al. [22] used the RBF method to build the response surfaces for the objective functions mixing index and pressure drop since it gave better accuracy ($R^2_{adj} > 0.9$) in particular for the mixing index response. The results of applying the NSGA-II on these response functions are shown in Fig. 4 for Re = 1, where Fig. 4a shows the plotting of 3200 iterations of designs points in the space mixing index vs. pressure drop where the Pareto front is clearly defined and Fig. 4b shows the validation of six samples of the Pareto front that were selected and evaluated with CFD. From Fig. 4a, the application gives an in-bounded set of optimum designs, i.e., the ranges of the two performance parameters are in the positive zone with coherent values (0–1 for mixing index and >0 for pressure drop), for the entire population generated by the genetic algorithm. These results confirm the ranges and levels of the design parameters in Table 1 were well selected for the DOE. In Fig. 4b, the difference in percentage between the CFD outcomes and the values predicted by the optimization method (dividing the difference between the CFD and the Pf values by the CFD value) is about 3% average in mixing index and 1% average in pressure drop, which are quite reasonable for the method employed and the trend of mixing performance vs. pressure drop in the designs is clearly predicted.

For Re = 1, the values of the design parameters of the six selected optimum designs of the Pareto front indicate that the geometric dimensions that vary significantly are only the height of the channel (h) and the depth of the groove (d_g) [22]. The aspect ratio of the channel is very influential on the mixing performance but the control of the pressure loss due to the multi-objective optimization do not let it reach the maximum possible value of 3.20 (see Table 1). Other design parameters do not change much along the Pf and they tend to the following optimum values: $d_g/h = 0.60$, $w_g/\lambda = 0.75$ and $b = 0.68$. One can see that very deep grooves do not necessarily improve mixing when the aspect ratio is also changing and what is important is the ratio d_g/h which, in this first part of the study,

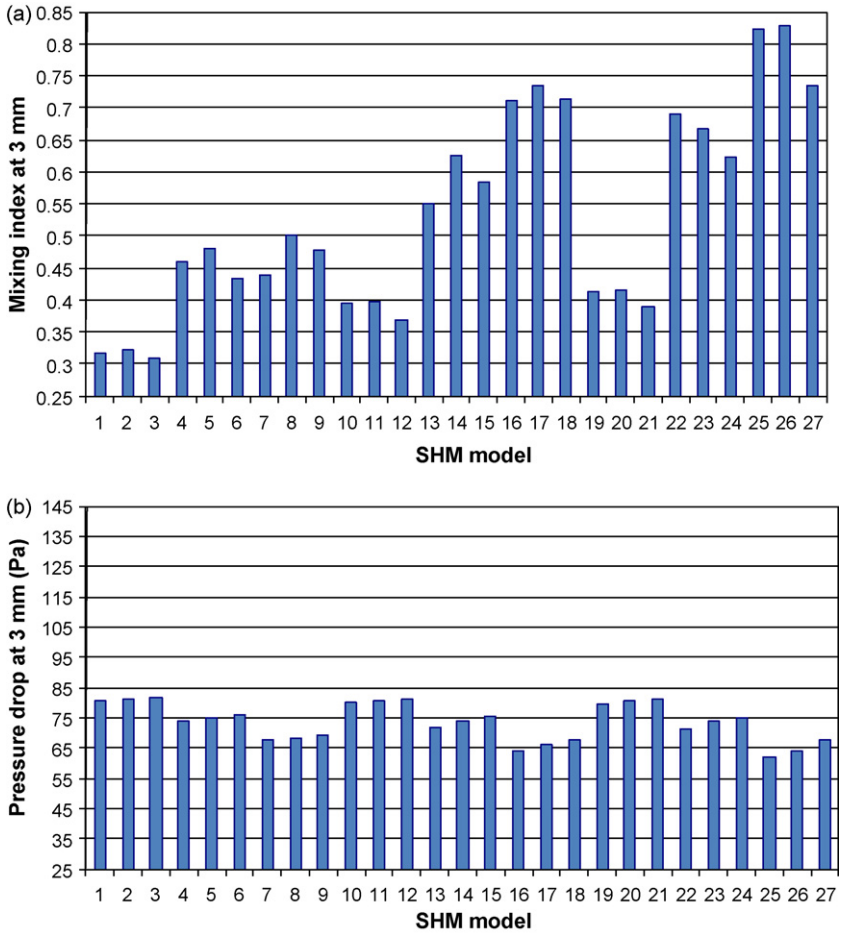

Fig. 7. Outcomes from CFD at the outlet of mixing channel of 27 DOE designs defined by Table 2 and OA L_{27} (Table 3), Re = 1: (a) mixing index and (b) pressure drop.

tends to be constant at 0.60. Also, the ratio w_g/λ adopts the highest possible value of 0.75 (see Table 1) showing that wide grooves promote higher flow rate inside them which generates the transversal flow that help mixing and also reduce the pressure loss in the system, which is in agreement with the main conclusion of Yang et al. [14]; parameter b tend to be around 0.68 which confirms the finding of Stroock et al. [8] that a value of 0.67 makes the transverse flow occupy most of the cross-sectional area of the mixing channel.

To continue with the second part of this study where two other design parameters: angle of the groove, θ, and number of grooves per half-cycle, N_g, are going to be evaluated with the optimization methodology, one optimum design of the six samples of the Pareto front (Fig. 4b) is selected as a reference design. This is actually the 19th design from 32 in the Pareto front and it gives the maximum mixing index. This optimum SHM design (from now on called RBFpf19 design) has the following geometric parameters: $w/h = 2.55$, $d_g/h = 0.60$, $w_g/\lambda = 0.75$ and $b = 0.69$, for the following geometric dimensions: $h = 78.5$ μm, $d_g = 47.1$ μm, $w_g = 75$ μm and $bw = 137.6$ μm, and it gives performance parameters outcomes of $Mi = 0.79$ and $\Delta p = 64.54$ Pa. Figs. 5 and 6 show the contours of some physical properties in the flow of Re = 1 in the RBFpf19 design. These contours will be used for analysis and comparison with contours in the optimum design that resulted from the second part of the optimization study.

In the second part of this study, the optimization methodology is applied to a set of designs defined by the design parameters shown in Table 2 and organized in the orthogonal array L_{27} (Table 3). This time, the RSM method was used to build the response surfaces, it gave better accuracy ($R^2_{adj} > 0.94$) for both objective functions which can be explained by the small range of the design parameters (see Table 2).

For the new design of experiments (Table 2 with Table 3), the mixing index and pressure drop outcomes from CFD at the outlet section of the mixing channel are shown in Fig. 7 for the 27 DOE designs at Re = 1. The variation of the mixing index is large between 0.3 and 0.83 approximately and it does not reveal clearly the effect of the design parameters when Fig. 7a is contrasted with the orthogonal array of experiments in Table 3. In Fig. 7b, the variation of pressure drop is between 61 and 81 Pa approximately; comparing Fig. 7b with the second column (factor B) of Table 3 one can notice the significant influence of the design variable w_g/λ, ratio of groove width to groove pitch, on the level of pressure drop in the mixing channel of the 27 DOE designs.

To evaluate the contribution that each level of a design parameter has on the S/N ratio of the mixing index, the mean of the S/N ratios of the experiments where the level of the design parameter is present in the OA L_{27} is calculated. The results are displayed in Fig. 8, where the positive slope of the curves indicates that increasing the value of the corresponding parameter results in a higher mixing index, and vice versa. From Fig. 8, the S/N analysis shows that for the ranges of the design parameters in Table 2, the highest mixing index at Re = 1 at the end of the optimization process is likely to be for the following values: parameter A, $d_g/h = 0.8$, parameter B, $w_g/\lambda = 0.75$ and parameter C, θ around 90°, whereas parameter D, N_g, does not show a value for which the mixing index is clearly higher. This analysis only shows the sensibility of mixing index to the design variables and it cannot give the optimum values of the design parameters since

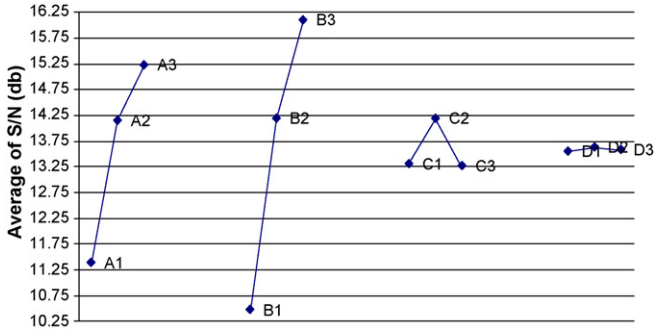

Fig. 8. Influence of design parameters on S/N ratio of mixing index for 27 DOE designs defined by Table 2 and OA L_{27} (Table 3), Re = 1.

the orthogonal array uses discrete values of design parameters (Table 2). The optimization with MOGA on response surfaces will explore a continuous space in the ranges defined for the design parameters.

Fig. 9 shows the results of the iterations from applying the NSGA-II on the response surfaces built with RSM method. For these results, the algorithm examined a continuous range (defined by the top and bottom values of parameters in Table 2) for all design parameters. Fig. 9a shows the plotting of 3200 iterations of designs points in the space mixing index vs. pressure drop and Fig. 9b shows the plotting of the 32 design nodes in the Pareto front. Fig. 10 also shows the results of the iterations of the NSGA-II searching the optimum designs but in this case the algorithm examined continuous range for the design parameters with the exception of the angle of the groove, θ, which was limited to discrete values with intervals of 5° in the range 70–110. For this case, Fig. 10a shows the plotting of 3200 iterations of designs points and Fig. 9b shows the plotting of 6 design nodes that resulted in the Pareto front (from the 32 nodes, some of them give exactly the same values of mixing index and pressure drop for the accuracy of computation, resulting in only 6 design nodes). A close comparison of the list of designs in the Pareto fronts depicted in Figs. 9 and 10 reveals that the 6 designs in the Pareto of Fig. 10 are included among the 32 designs of the Pareto of Fig. 9. This reveals the consistency of the algorithm convergence.

Therefore, the five designs of Pareto front in Fig. 10 that give higher mixing index are selected for the validation of the predicted response outcomes with numerical simulations. In Fig. 11, the CFD outcomes are shown with the values of corresponding design nodes of the Pareto front; the average differences in percentage between absolute values is 0.55% in mixing index and 0.14% in pressure drop with maximum absolute differences of 1.13% in mixing index in the second design node and 0.31% in pressure drop in the third design node (the order is taken from Fig. 11, from low to high pressure

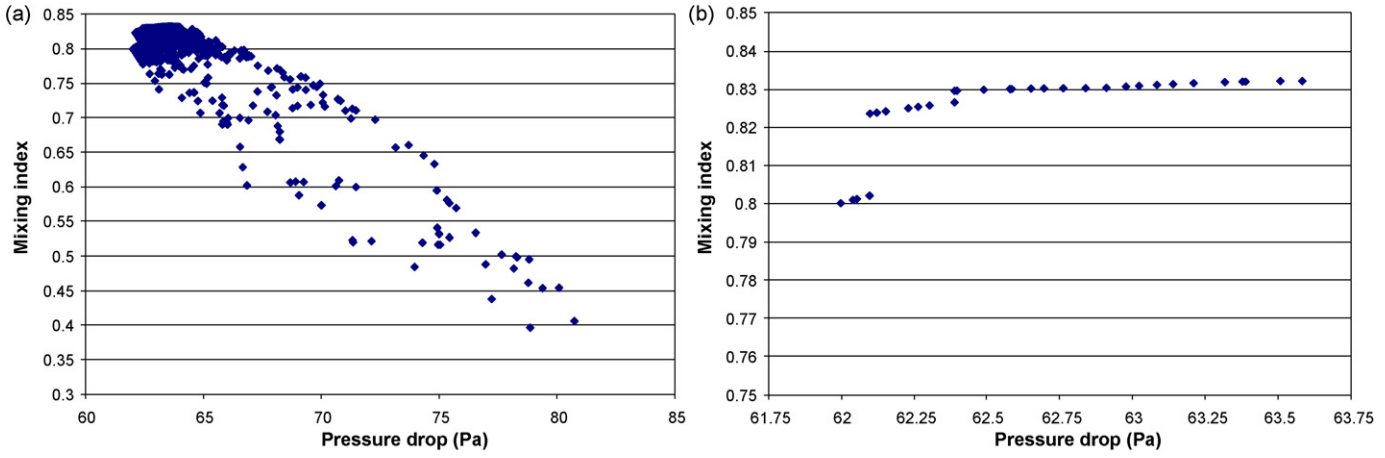

Fig. 9. Results from application of NSGA-II algorithm (using continuous values for optimization of design parameter θ, angle of the groove) on response surfaces built by RSM method: (a) scatter of iterations history and (b) scatter of designs on the Pareto front.

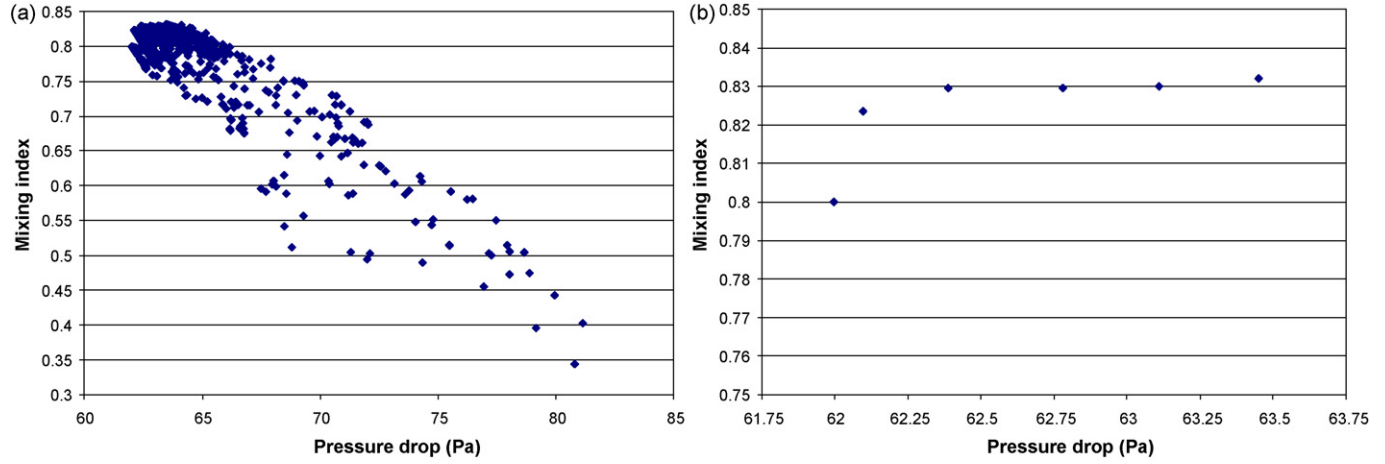

Fig. 10. Results from application of NSGA-II algorithm (using discrete values for optimization of design parameter θ, angle of the groove) on response surfaces built by RSM method: (a) scatter of iterations history and (b) scatter of designs on the Pareto front.

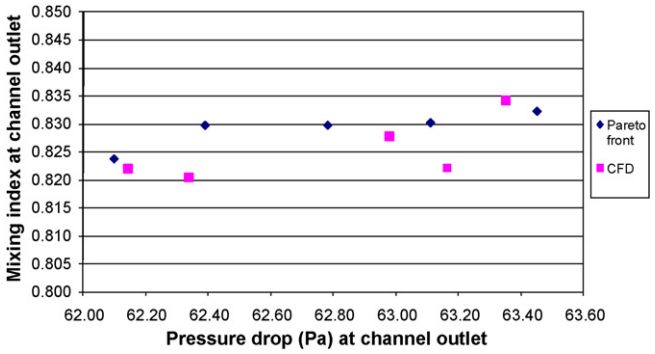

Fig. 11. Mixing index vs. pressure drop in five selected designs of the Pareto front from optimization on RSM surfaces and corresponding CFD outcomes.

drop). These very small differences are mainly due to the accuracy of the response surfaces. Fig. 11 shows there is an increment in pressure drops along the five designs but the trend in mixing index is not evident what can be due to computational errors considering the small range of variation of mixing index between 0.8237 and 0.8322 in the Pareto front.

Table 4
Design parameters of Pf designs from optimization on RSM surface, Re = 1.

Pf design	Params.			
	A (d_g/h)	B (w_g/λ)	C (θ°)	D (N_g)
RSM pf1	0.8	0.75	70	6
RSM pf2	0.8	0.75	70	5
RSM pf3	0.8	0.75	75	6
RSM pf4	0.8	0.75	75	5
RSM pf5	0.8	0.75	80	6

Table 4 shows the values of the design parameters and Table 5 shows the corresponding geometric dimensions of the five selected designs of the Pareto front. From Table 4 one can conclude that higher values of ratios d_g/h and w_g/λ increase mixing and reduce pressure loss when the aspect ratio is fixed. In the first part of the study (design of experiments with Tables 1 and 3), the aspect ratio changed during the optimization and it apparently controls the variation of the d_g/h ratio which tends to 0.60 in the Pareto

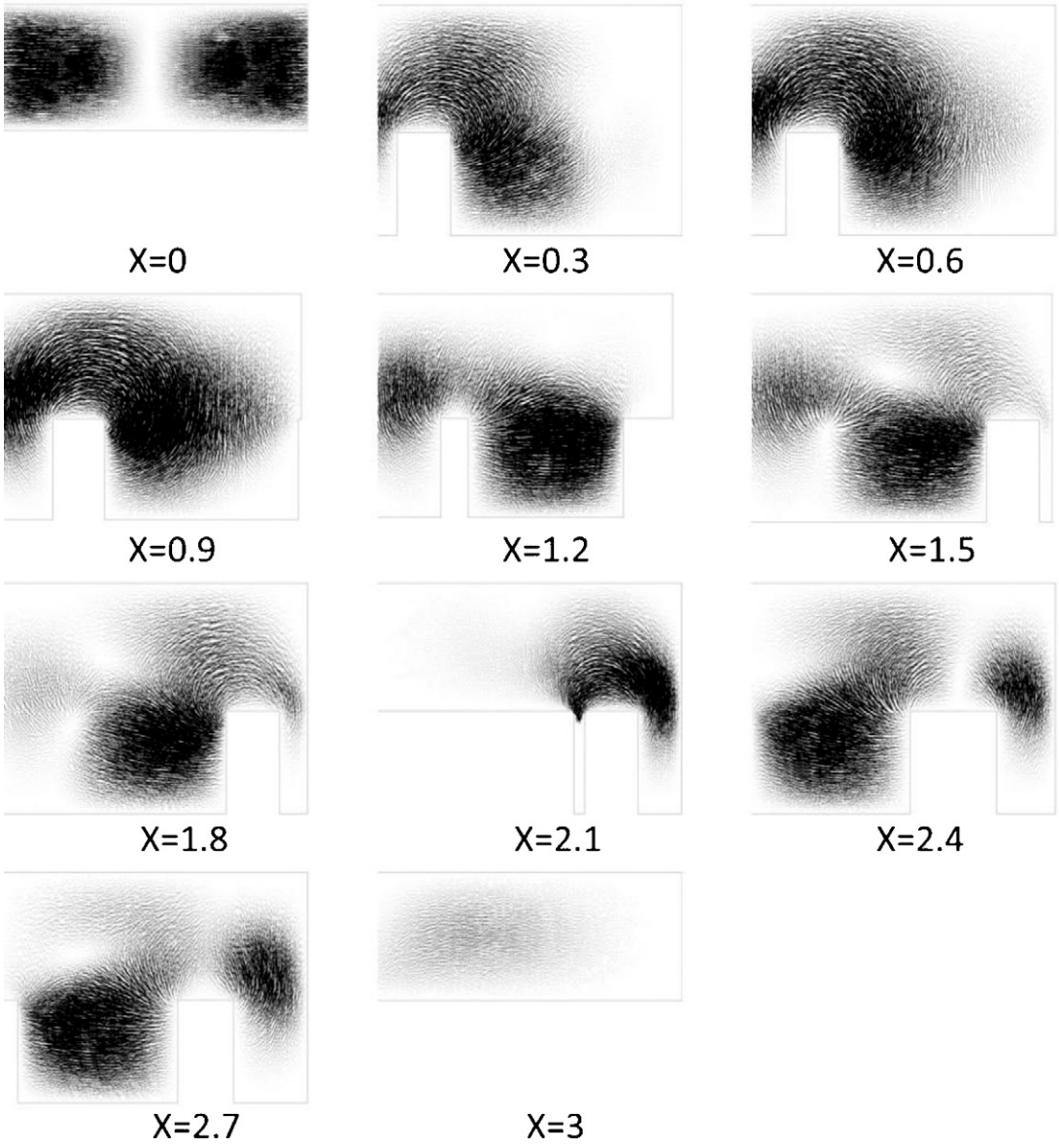

Fig. 12. Vector plots on cross-section planes of mixing channel of optimum design RSM pf5 from second part of optimization study.

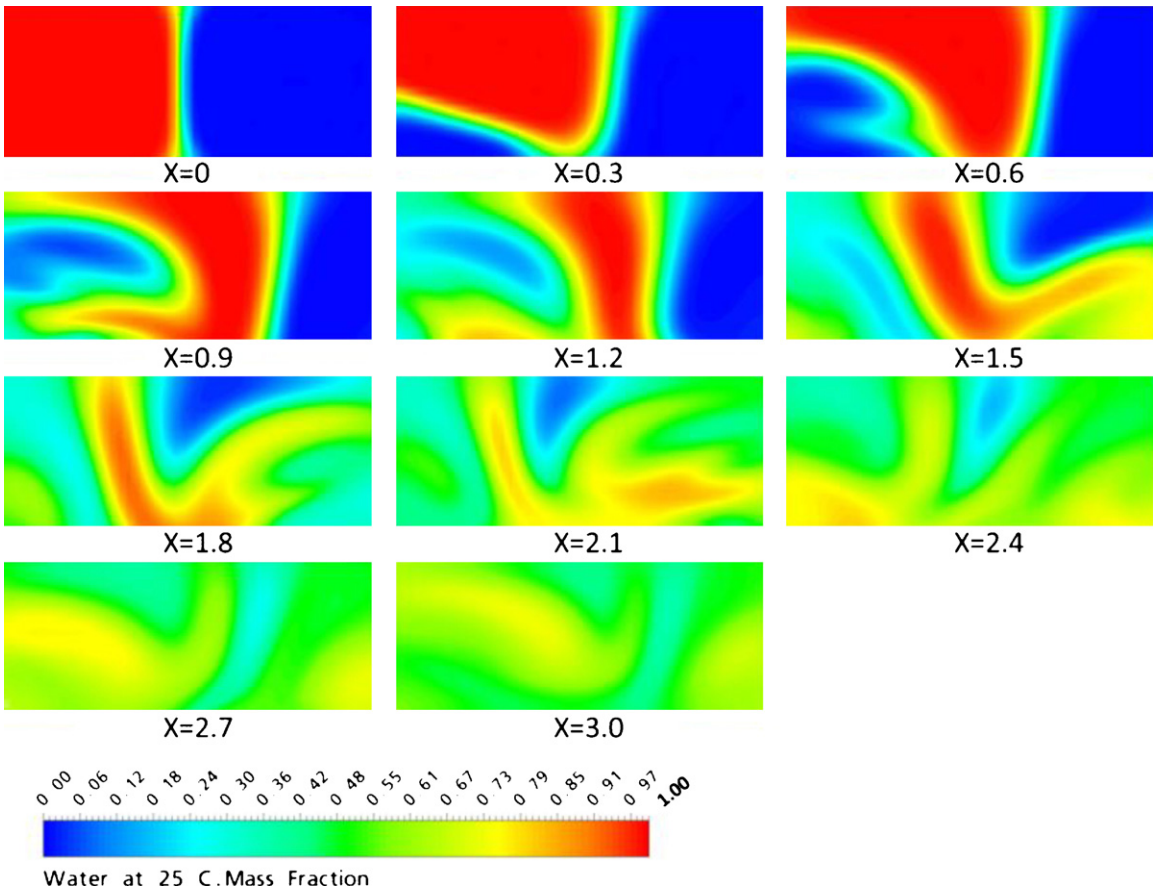

Fig. 13. Mass fraction contours on cross-section planes of mixing channel of optimum design RSM pf5 from second part of optimization study.

front. The influence of parameter θ on mixing index is not explicit from Table 4 and Fig. 11 but it is clear that pressure drop increases with an increase in the angle of the groove, in the Pareto front of Fig. 9b the value of parameter θ goes from 70 to 81.02 with pressure drop increasing from 62 to 63.6 Pa. These values are very similar to those obtained in the Pareto front of Fig. 10b although in this case the optimization employs discrete values of parameter θ. The influence of parameter N_g on mixing index and pressure drop is not relevant compared to the other three design parameters, what can be explained by the small range, 5–7, used in this study, although N_g is equal to 6 in 20 of the 32 designs in the Pareto front of Fig. 9b.

The effect of the parameters d_g/h and w_g/λ can be seen in Fig. 12. This figure shows the vector plots on cross-section planes every 0.3 mm along the mixing channel of the optimum design, the one that gives the highest mixing index, in the Pareto front of Fig. 10a (design RSM pf5 in Table 5). The formation of vortices is promoted by the angle of the groove (whose value is 80° from the optimization study) that creates a transverse flow which rotates the stream of fluids throughout the length of the mixing channel. The vortices cover large part of the cross-section of the channel and the highest values in their optimization range adopted by parameters d_g/h and w_g/λ results in the formation of a strong main vortex that enhances mixing of the fluids.

Optimum design RBFpf19 from the first part of the optimization study [22] was taken as the reference design to perform the second part of the study that resulted in the optimum design RSM pf5 (Tables 4 and 5). The comparison of geometries of designs RBFpf19 and RSM pf5 is summarized in Table 6.

Table 6 reveals that the whole optimization procedure for a total of six designs variables gives an optimum design once completed the second part of the study; the differences between first part optimum design RBF pf19 and second part optimum design RSM pf5 are in the ratio of groove depth to channel height, d_g/h, and the angle of the groove, θ. The parameter d_g/h, that changes from 0.6 in RBF pf19 to 0.8 in RSM pf5, is the design variable whose effect on mixing is more significant to redefine the optimum design in the second part of this study; an increase in d_g/h increases mixing index, result that is consistent with previous studies [14,16,18], and reduces pressure drop. On other hand, an increase in θ increases pressure drop, what is evident from Tables 4 and 5, and the effect of θ on mixing index

Table 5
Geometric dimensions (μm) of Pf designs from optimization on RSM surface, Re = 1 and corresponding values of mixing index and pressure drop at the outlet section.

Pf design	Dimens.					
	h	d_g	w_g	bw	Mi	Δp (Pa)
RSM pf1	78.46	62.77	75	137.6	0.8220	62.14
RSM pf2	78.46	62.77	75	137.6	0.8204	62.34
RSM pf3	78.46	62.77	75	137.6	0.8278	62.98
RSM pf4	78.46	62.77	75	137.6	0.8221	63.16
RSM pf5	78.46	62.77	75	137.6	0.8342	63.35

Table 6
Geometric dimensions (μm) of Pf designs from first (RBF pf19) and second (RSM pf5) parts of the optimization study, Re = 1 and corresponding values of mixing index and pressure drop.

Pf design	Dimens.							
	h	d_g	w_g	bw	θ°	N_g	Mi	Δp (Pa)
RBF pf19	78.46	47.08	75	137.6	90	6	0.79	64.54
RSM pf5	78.46	62.77	75	137.6	80	6	0.83	63.35

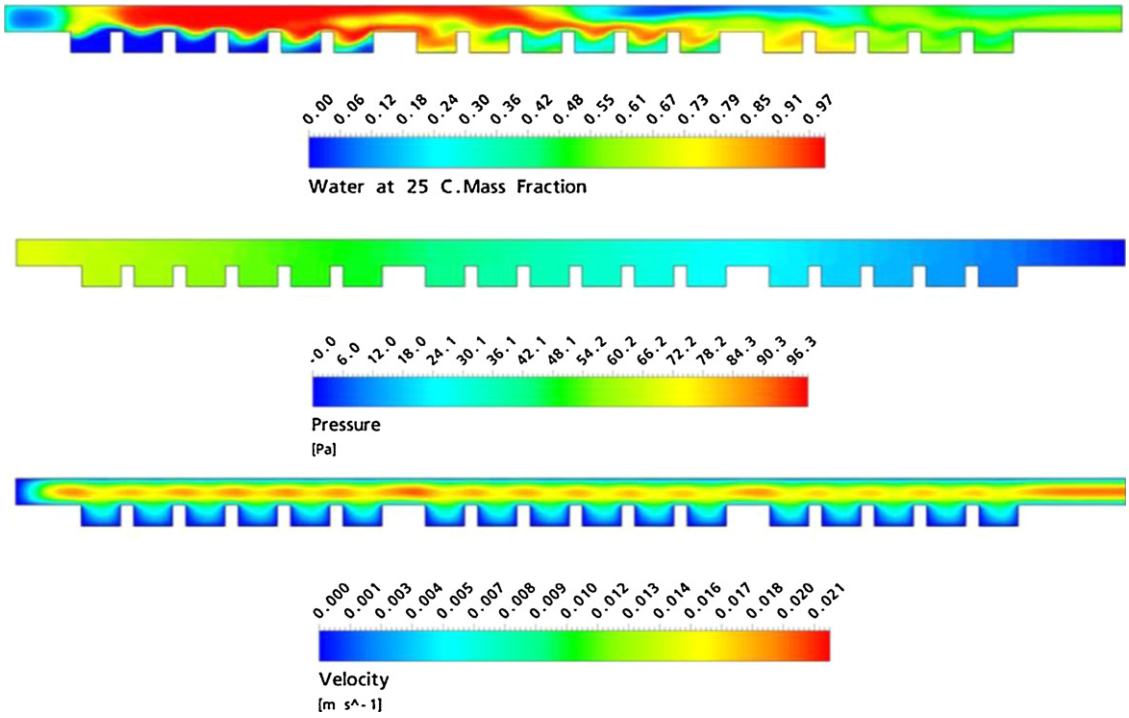

Fig. 14. Mass fraction, pressure and velocity contours on symmetrical vertical plane of mixing channel of optimum design RSM pf5 from second part of optimization study.

is not explicit; from information in Tables 4 and 5, the control of parameter θ during the second part of the optimization shows mixing increases slightly when θ increases from 70 to 80°, result that is consistent with the Taguchi's S/N ratio analysis (Fig. 8) that found θ has mild impact on mixing index and estimated its optimum value would be around 90°.

Fig. 13 shows the mass fraction contours on several cross-sections of the mixing channel and Fig. 14 shows the contours of mass fraction, pressure and velocity on a symmetrical vertical plane crossing longitudinally the mixing channel of the optimum design RSM pf5. Contours in Figs. 13 and 14 can be compared to the contours in Figs. 5 and 6, respectively, which correspond to design RBF pf19.

In Figs. 5 and 13, the contours of mass fraction at cross-sections every 0.3 mm of the mixing channel (the groves are not included) appear quite similar until $x = 2.1$ mm where some different patterns can be distinguished. The similarity of the flows at Re = 1 is due to the several geometric features both designs have in common (see Table 6). In Figs. 6 and 14, the mass fraction contours show how ethanol occupy most of the cross-section of the grooves of the first half-cycle whereas water occupy most of the mixing channel on the longitudinal symmetry plane because it is convectively forced to fill the spaces ethanol left for migrating into the grooves; the vertical motion induced by the grooves in the channel can be identified by the zone adjacent to the top wall of the channel between the first and second cycles which is occupied by ethanol that has rolled up in the channel, this is more evident in the case of RBF pf19 (Fig. 6). Mass fraction distribution (flow) appear more perturbed in the case of RSM pf5 (Fig. 14) from the beginning of the second half-cycle towards the outlet of the channel. There is not major difference in the patterns of contours of pressure and velocity on the symmetrical vertical plane of the channels; contours of velocity show how flow accelerates over the ridges between grooves due to the reduction of the cross-section area in this zones and the presence of stagnation zones (dead zones) in about third (RBF pf19) and fourth (RSM pf5) the cross-section of the grooves, which cannot be compared directly considering the different values of d_g/h of the two designs. Formation of dead volumes against mixing performance is directly affected by this design variable and its evaluation using different fluids and flow conditions (Reynolds number) is not in the scope of this paper.

5. Conclusions

A truly optimization methodology for micromixers based on the integration of CFD and numerical optimization techniques (DOE, SM and MOGA) has been employed for the multi-objective optimization of the geometries of a grooved micromixer, the staggered herringbone micromixer (SHM), to maximize mixing index and minimize pressure drop in the channel. In the first part of the optimization study, the conclusions of Cortes-Quiroz et al. [22] have been reviewed and the optimum design that resulted from the optimization of four design parameters (aspect ratio of the mixing channel, w/h, ratio of groove depth to channel height, d_g/h, ratio of groove width to groove pitch, w_g/λ, and the asymmetry factor of groove, b) was taken as reference design for optimization of two additional design parameters: angle of the groove, θ, and number of grooves per half-cycle, N_g (Table 2).

The methodology process cycle is repeated for the second part of the optimization study. The DOE method is used to create experimental tables of 27 designs based on the reference design. Detailed analysis of signal-to-noise ratios for these designs at Re = 1 (Fig. 8) shows that two design parameters have significant effect on mixing index: d_g/h and w_g/λ, whereas the effect of θ was not explicit and N_g appeared not significant for mixing in the interval (see Table 2) used. Two surrogate modelling techniques have been employed, radial basis function (RBF) and response surface model (RSM). The RBF method gave very accurate approximation of the response functions in the first part of the optimization study whereas the RSM was more accurate in the second part due to the relative small range used for design parameters. Applying MOGA on the response surfaces, the Pareto front of mixing index vs. pressure drop is obtained. The Pareto front shows the trend and quite approximated values of mixing index and pressure drop in designs that respond to

the optimization goal. Five designs in the Pareto front that predict higher mixing index were validated by CFD and the comparison of the results shows maximum absolute difference of 1.13% in mixing index and 0.31% in pressure drop which reveal the methodology can give good accuracy for the prediction of optimum designs for which the accuracy of the response surface is critical.

The optimum designs (high mixing performance with lowest possible pressure drop) show the significant impact of parameter w_g/λ on mixing, increase in the width of the grooves increases the mixing performance in the SHM design. Optimum value of parameter w_g/λ of 0.75 corresponds to the maximum value in the range defined for this study (which was limited considering materials and fabrication issues); this is valid when optimizing with a variable aspect ratio or a fixed aspect ratio. Parameter d_g/h is also found to have effective influence on performance parameters, increase in d_g/h increases mixing index and reduces pressure drop. Optimum value of parameter d_g/h of 0.60 corresponds to the optimization with variable aspect ratio and it reaches the maximum value in its range, 0.8, when optimizing with fixed aspect ratio; this shows the shared effect these parameters have on the performance parameters, in particular the aspect ratio was found the most influential on pressure drop from the first part of the study. The effect of parameter θ on the performance of the micromixer is not as explicit as the previous parameters; it is found that an increase in θ increases pressure drop and mixing increases slightly when θ increases from 70 to 80° what is explained by the presence of secondary flows in more transversal direction. In general, parameter θ has less significant impact on mixing than parameters w_g/λ and d_g/h. The definition of a groove pitch in direction perpendicular to the walls of grooves makes geometric dimensions θ and w_g to be independent of each other, what is important for the optimization and evaluation of parameters w_g/λ and θ without much confounding of their effects on performance of the micromixer; this is critical and, to the knowledge of the authors, this definition of groove pitch, λ, is applied for the first time in this paper in a study that includes parameter θ in the optimization of SHM design. Finally, the influence of parameter N_g on mixing index and pressure drop is found not as relevant as the other three design parameters, what can be explained by the small range, 5–7, used in this study.

Acknowledgments

This work was supported by a Dorothy Hodgkin Postgraduate Award (DHPA) of the United Kingdom and by Ebara Research Co. Ltd. of Japan.

References

[1] H.A. Stone, A.D. Stroock, A. Ajdari, Engineering flows in small devices: microfluidics toward a lab-on-a-chip, Annu. Rev. Fluid. Mech. 36 (2004) 381–411.
[2] C. Hansen, S.R. Quake, Microfluidics in structural biology: smaller, faster, better, Curr. Opin. Struct. Biol. 13 (2003) 538–544.
[3] W. Ehrfeld, V. Hessel, H. Lowe, Microreactors, Wiley-VCH, Boston, 2000.
[4] D.R. Reyes, D. Iossifidis, P.A. Auroux, A. Manz, Micro-total analysis systems. 1. Introduction, theory and technology, Anal. Chem. 74 (2002) 2623–2636.
[5] J.M. Ottino, The Kinematics of Mixing: Stretching, Chaos and Transport, Cambridge University Press, Cambridge, 1989.
[6] N. Nguyen, Z. Wu, Micromixers—a review, J. Micromech. Microeng. 15 (2005) R1–R16.
[7] V. Hessel, H. Lowe, F. Schonfeld, Micromixers, a review on passive and active mixing principles, Chem. Eng. Sci. 60 (2005) 2479–2501.
[8] A.D. Stroock, S.K.W. Dertinger, A. Ajdari, I. Mezić, H.A. Stone, G.M. Whitesides, Chaotic mixer for microchannels, Science 295 (2002) 647–651.
[9] A.D. Stroock, G.J. McGraw, Investigation of the staggered herringbone mixer with a simple analytical model, Phil. Trans. R. Soc. Lond., Ser. A 362 (1818) (2004) 971–986.
[10] Y.Z. Liu, B.J. Kim, H.J. Sung, Two-fluid mixing in a microchannel, Int. J. Heat Fluid Flow 25 (2004) 986–995.
[11] J. Aubin, D.F. Fletcher, J. Bertrand, C. Xuereb, Characterization of the mixing quality in micromixers, Chem. Eng. Technol. 26 (12) (2003) 1262–1270.
[12] J. Aubin, D.F. Fletcher, C. Xuereb, Design of micromixers using CFD modelling, Chem. Eng. Sci. 60 (8–9) (2005) 2503–2516.
[13] T.G. Kang, T.H. Kwon, Colored particle tracking method for mixing analysis of chaotic micromixers, J. Micromech. Microeng. 14 (7) (2004) 891–899.
[14] J.-T. Yang, K.-J. Huang, Y.-C. Lin, Geometric effects on fluid mixing in passive grooved micromixers, Lab Chip 5 (10) (2005) 1140–1147.
[15] C. Li, T. Chen, Simulation and optimization of chaotic micromixer using lattice Boltzmann method, Sens. Actuators B 106 (2005) 871–877.
[16] D.G. Hassel, W.B. Zimmerman, Investigation of the convective motion through a staggered herringbone micromixer at low Reynolds number flow, Chem. Eng. Sci. 61 (2006) 2977–2985.
[17] N.S. Lynn, D.S. Dandy, Geometrical optimization of helical flow in grooved micromixers, Lab Chip 7 (2007) 580–587.
[18] M.A. Ansari, K.-Y. Kim, Shape optimization of a micromixer with staggered herringbone groove, Chem. Eng. Sci. 62 (2007) 6687–6695.
[19] M.K. Singh, T.G. Kang, H.E.H. Meijer, P.D. Anderson, The mapping method as a toolbox to analyze, design and optimize micromixers, Microfluid. Nanofluid. 5 (3) (2008) 313–325.
[20] T.G. Kang, M.K. Singh, T.H. Kwon, P.D. Anderson, Chaotic mixing using periodic and aperiodic sequences of mixing protocols in a micromixer, Microfluid. Nanofluid. 4 (6) (2008) 589–599.
[21] C.A. Cortes-Quiroz, M. Zangeneh, A. Goto, A multi-objective analysis and optimization methodology for the design of passive micromixers based on their own topology, in: Proceedings of the AIChE Annual Meeting, IMRET-10 International Conference on Microreaction Technology, New Orleans, US, 2008, p. 2008.
[22] C.A. Cortes-Quiroz, M. Zangeneh, A. Goto, On multi-objective optimization of geometry of staggered herringbone micromixer, Microfluid. Nanofluid. 7 (1) (2009) 29–43.
[23] CFX 10.0 User Manual, ANSYS Europe Ltd., 2007.
[24] Gridgen 15. 1 User Manual, Pointwise Inc., 2006.
[25] P.V. Danckwerts, The definition and measurement of some characteristics of mixtures, Appl. Sci. Res. A 3 (1952) 279–296.
[26] G. Taguchi, Systems of Experimental Design, vols. 1 and 2, Kraus International, New York, 1987.
[27] R.H. Myers, Response surface methodology—current status and future direction, J. Qual. Technol. 31 (1) (1999) 30–74.
[28] R.L. Hardy, Multiquadric equations of topography and other irregular surfaces, J. Geophys. Res. 176 (1971) 1905–1915.
[29] E.J. Kansa, Multiquadrics - A scattered data approximation scheme with applications to computational fluid-dynamics: I. Surface approximations and partial derivative estimates, Comput. Math. Appl. 19 (8–9) (1990) 127–145.
[30] R.H. Myers, D.C. Montgomery, Response Surface Methodology: Process and Product Optimization Using Designed Experiment, Wiley, New York, 1995.
[31] C. Yiu, M. Zangeneh, A 3D automatic optimization method for turbomachinery blade design, AIAA J. Propul. Power 16 (6) (2000) 1174–1181.
[32] G.N. Vanderplaats, Numerical Optimization Techniques for Engineering Design with Applications, McGraw-Hill Book Company, New York, 1984.
[33] K. Deb, A. Agrawal, T. Pratap, T. Meyarivan, A fast and elitist multi-objective genetic algorithm for multi-objective optimization: NSGA-II, in: Proceedings of the Parallel Problem Solving from Nature VI Conference, Paris, France, 2000, pp. 849–858.